

Optics Letters

Cooke–Triplet tweezers: more compact, robust, and efficient optical tweezers

TIM STANGNER,¹  TOBIAS DAHLBERG,¹ PONTUS SVENMARKER,¹  JOHAN ZAKRISSON,¹
KRISTER WIKLUND,¹ LENE B. ODDERSHEDE,²  AND MAGNUS ANDERSSON^{1,*} 

¹Department of Physics, Umeå University, 901 87 Umeå, Sweden

²The Niels Bohr Institute, University of Copenhagen, Blegdamsvej 17, 2100 Copenhagen, Denmark

*Corresponding author: magnus.andersson@umu.se

Received 13 February 2018; accepted 20 March 2018; posted 26 March 2018 (Doc. ID 323138); published 19 April 2018

We present a versatile three-lens optical design to improve the overall compactness, efficiency, and robustness for optical tweezers based applications. The design, inspired by the Cooke–Triplet configuration, allows for continuous beam magnifications of 2–10 \times , and axial as well as lateral focal shifts can be realized without switching lenses or introducing optical aberrations. We quantify the beam quality and trapping stiffness and compare the Cooke–Triplet design with the commonly used double Kepler design through simulations and direct experiments. Optical trapping of 1 and 2 μm beads shows that the Cooke–Triplet possesses an equally strong optical trap stiffness compared to the double Kepler lens design but reduces its lens system length by a factor of 2.6. Finally, we demonstrate how a Twyman–Green interferometer integrated in the Cooke–Triplet optical tweezers setup provides a fast and simple method to characterize the wavefront aberrations in the lens system and how it can help in aligning the optical components perfectly. © 2018 Optical Society of America

OCIS codes: (220.1000) Aberration compensation; (220.3620) Lens system design; (350.4855) Optical tweezers or optical manipulation.

<https://doi.org/10.1364/OL.43.001990>

Since the first publication of a single-beam gradient force trap by Ashkin and coworkers in 1986 [1], optical tweezers (OT) are now standard equipment in many laboratories worldwide and have resulted in great discoveries in several biological systems [2–7]. Besides their biophysical application, it was recently demonstrated that optical trapping is a mechanism allowing for realization of 3D displays [8]. For this to materialize in everyday life, however, it is necessary to develop very compact, robust, and highly efficient OT.

A standard OT is created by a laser beam, a lens system to control the laser beam, and a high numerical aperture (NA) microscope objective to focus the light into a sample chamber. A common and widely used lens system to control the beam properties is a four-lens design that is commonly denoted as the

double Kepler (DK). In the DK setup, the first lens pair magnifies the laser beam to a desired diameter, and the second controls the beam divergence to adjust the height of the trap (axial position) in the sample chamber [9]. If the lateral trap position needs additional tuning, a third lens pair with lenses of equal focal lengths must be introduced into the beam path [10].

However, building an optical trap based on such a three-lens-pair DK design results in three direct limitations: (i) a fixed magnification. To create an efficient trap that can work at low laser intensities, thereby minimizing photodamage to the sample, a filling ratio $\alpha = 0.8 - 0.9$ is recommended [11,12]. Here, we denote α as the ratio between the incoming beam diameter $2\omega_0$ (at which the intensity drops to $1/e^2$ of the center value of the Gaussian beam profile) and the exit pupil diameter of the used objective $D_{\text{NA}} = 2f_{\text{obj}} \cdot \text{NA}$ (f_{obj} = focal length of objective, NA = numerical aperture of objective). If an objective with a different magnification, a different NA, or from a different supplier is used, the optimal α changes. Thus, to retrieve the optimal value of α , the beam diameter must be adjusted. As a consequence, the lens pair used for beam magnification must be modified and realigned. The same problem arises if the laser source is replaced with a new laser that has a different initial beam diameter or beam divergence. (ii) Setup size and alignment effort. To achieve full control of the filling ratio α and the axial and lateral trap position using the DK, it requires at least three lens pairs with an average combined focal length for each pair $f = 200\text{--}350$ mm, resulting in an average total beam path of ≈ 825 mm [9]. Realizing such long beam paths usually involves several mirrors or beamsplitter cubes to steer the beam on the optical table, thus increasing the alignment effort and reducing the system stability due to drifts (mechanical, temperature). Smaller OT setups can be realized by reducing the focal length of the beam steering lens pairs (axial, lateral). However depending on the beam diameter used, highly curved lenses with short focal lengths are likely to introduce spherical aberrations (SAs), which are known to reduce the trapping quality [13,14]. (iii) Reduced laser pointing stability. For a high-precision OT it is crucial to reduce laser pointing instabilities to a minimum as they lead to lateral shifts in the trap position. Common sources for this instability are a poor

trapping laser quality, but also focusing at high laser intensities using lenses can lead to a change in refractive index of the surrounding atmosphere, causing pointing instabilities [10].

To address issue (i) a three-lens Galilean telescope, a combination of two negative lenses and one positive, was used in literature to achieve a continuous beam magnification without the need to replace lenses [11]. However, using this approach for OT design would require two additional lens pairs for axial and lateral trap position control, leaving issues (ii) and (iii) unsolved.

In this Letter, we show that by using a Cooke–Triplet (CT) lens design [15], limitations (i)–(iii) can be overcome by using only three singlet lenses. The special lens combination of the CT gives us full control to continuously change the beam magnification and the axial and lateral trap position in the measurement chamber without introducing optical aberrations such as SA, astigmatism, or coma [16]. To quantify, investigate, and compare aberrations in the CT and DK setups we introduce a Twyman–Green interferometer [17] into the OT setup [18] and conduct ray-tracing simulations. In addition, we show that the CT generates an equally strong trap compared to the DK design for trapping of 1 and 2 μm polystyrene (PS) particles. We also provide a Matlab program to estimate the optimal distances between the CT lenses to achieve parallel light as output.

To measure optical aberrations and trap stiffnesses at the same time, we combine a Twyman–Green interferometer and an OT setup (Fig. 1). A CW laser beam (1064 nm, $\varnothing_{\text{Beam}} = 1$ mm, Rumba, 05-01 Series, Cobolt AB) is divided by a beamsplitter cube (BSC, Thorlabs) into two beams with equal intensity and guided onto a mirror (M1) and through the laser beam control lenses. The latter is realized by either a DK telescope (DK1; $f_1 = 60$ mm, $f_2 = 250$ mm, $f_3 = 175$ mm, $f_4 = 175$ mm, Thorlabs) or a CT ($f_1 = 60$ mm, $f_2 = -15$ mm, $f_3 = 250$ mm, Thorlabs) lens design. The movable mirror (M2) is either used to reflect the trapping beam back to the BSC to form an interferogram at the beam profiler camera (Pyrocam IIIHR, Ophir Optronics) or to guide it into the microscope objective (100 \times , Oil Iris, NA = 1.3,

$f_{\text{obj}} = 1.8$ mm, 0.17/ ∞ , Olympus) to create the optical trap. The exit pupil diameter of the objective is $D = 4.68$ mm.

To compare aberrations and trap stiffness of the DK1 and CT setups, we magnify the laser beam by a factor of ~ 4 resulting in a beam diameter of $2\omega_0 \approx 4$ mm. To ensure parallel light output at the fourth lens (DK1: L4) and third lens (CT: L3), we use the Twyman–Green interferometer to align the lenses (separation distance and tilt) with high precision by analyzing the respective interferograms. Additionally, we measure the beam diameter $2\omega_0$ at two positions after the last lens. To measure the trap stiffness, we use a probe laser operating at 632.8 nm (HeNe-laser, 1137 Uniphase, Manteca). The light from the probe laser is aligned with the trap laser using a dichroic BSC mounted in the microscope, and the forward scattered light of the trapped object is collected by the condenser and imaged onto a 2D position sensitive detector (L20 SU9, Sitek Electro Optics) [19]. For representative purposes we do not show the probe laser in the figure. Afterward, we calculate the power spectral density from the detector signal and fit the data to retrieve the trap stiffness in lateral directions x and y [20,21].

Before measuring aberrations experimentally, we perform ray-tracing simulations in OpticStudio (Version 17.5, Zemax) to highlight the ability of a compact CT to provide continuous beam magnification without changing lenses or introducing optical aberrations. Further, we scrutinize the effect of system miniaturization on wavefront aberrations by simulating two DK telescopes using different focal lengths for the beam divergence control lens pair (Fig. 1, DK1: $f_{3,4} = 175$ mm; DK2: $f_{3,4} = 60$ mm). Since each DK lens system can only produce one fixed beam magnification, we use various lens combinations for the beam magnification lens pair to realize beam diameters between 2 and 10 mm. A summary of these lens pairs, the corresponding OpticStudio files, and a custom-made Matlab program to estimate the lens distances for CT lenses to produce parallel light output for a predefined beam magnification are published in [22]. To assess the wavefront aberrations in OpticStudio, we set the wavelength to 1064 nm and the initial beam diameter to 1 mm, thus reproducing the specifications of our laser. Further, rays from the monochromatic light source propagate along the optical axis of the lens system, entering all lenses centered and without tilt. After the rays in the beam propagate twice through the entire optical lens system, a virtual detector records the wavefront and calculates the wavefront aberrations.

The simulation results show first that the CT lens design can realize continuous beam magnifications between 2 \times and 10 \times [Fig. 2(a)]. Second, all tested systems show only SA (Seidel wavefront aberrations coefficient $W040$ spherical), leaving all other primary aberrations negligible. Third, independent of the simulated beam diameter, the CT has superior performance by showing the least amount of SA, followed by the DK designs DK1 and DK2. In average, the CT reduces SA by a factor of 9.2 ± 0.9 (mean \pm standard error [SE]) and 186 ± 20 (mean \pm SE) compared to DK1 and DK2, respectively. In this context, we emphasize that the DK1 (long focal length divergence control) shows 20 \times less aberrations than the DK2 (short focal length divergence control). This increase in SA shows the problem in miniaturizing a DK lens system. A reduction of the DK lens system length by a factor of 1.5 (DK1/DK2), for a given beam magnification [Fig. 2(b)], results

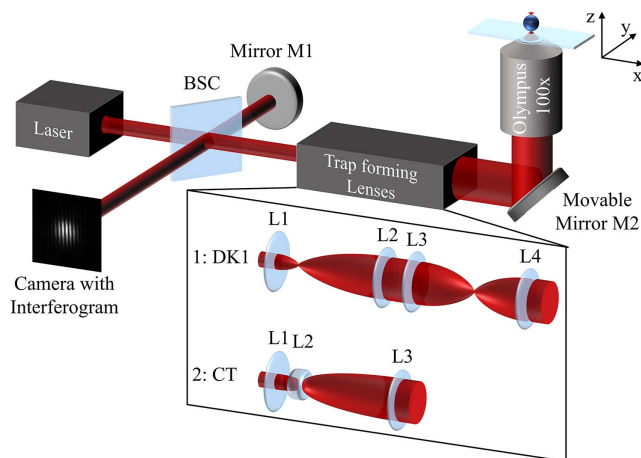


Fig. 1. Schematic of the combined Twyman–Green interferometer and OT setup. BSC, beamsplitter cube; DK1, double Kepler lens system; CT, Cooke–Triplet lens system; L1–L4, Lens 1–4. For trapping we use an immersion oil with $n = 1.518$ (Olympus). The laser power is measured to 37 mW before entering the objective. The filling ratio is $\alpha = 0.84$.

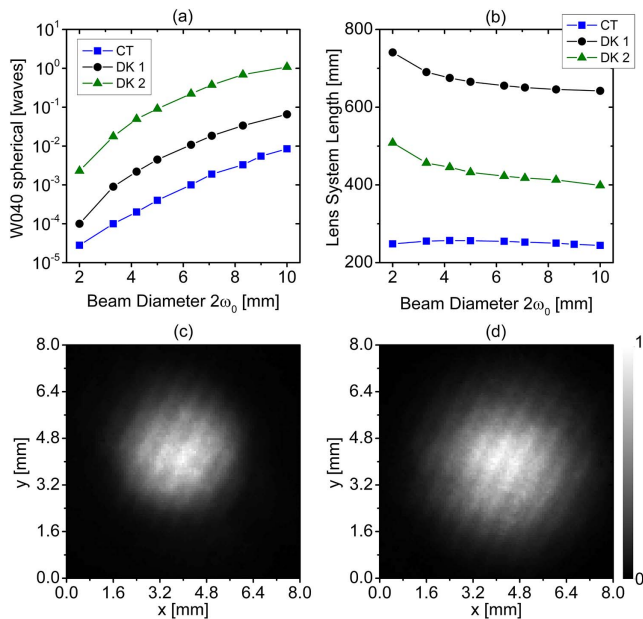


Fig. 2. OpticStudio simulations to determine (a) the Seidel wavefront aberrations coefficient for SA (W_{040} spherical) as a function of the beam diameter $2\omega_0$ for the CT (blue squares), DK1 (black spheres), and DK2 (green triangles) lens design. (b) Total lens system length for the setups used in (a) as a function of beam diameter. (c) Measured interferogram for the DK1 and (d) the CT for a beam diameter of $2\omega_0 \approx 4$ mm.

in a significant increase of SA. Furthermore, the lens system length for DK1 (DK2) depends strongly on the desired beam magnification, ranging from 642 to 741 mm (399–508 mm). In contrast, the length of the CT stays almost the same, varying only 13 mm among all beam magnifications [Fig. 2(b)]. Consequently, besides its compact design (1.7 \times shorter than DK2; 2.6 \times shorter than DK1), the CT is able to realize a broad range of beam diameters with only minor changes in the positions of lens L2 and L3 (Fig. 1), keeping the setup alignment preserved.

To estimate the impact on wavefront aberrations if either the axial or the lateral trap position is modified, we conduct another set of ray-tracing simulations. To adjust the axial trap position inside a sample chamber (fixed lateral position), the light entering the objective is slightly focused via the divergence control lens pair (DK1, DK2: L3 and L4; CT: L2 and L3). Again, our ray-tracing simulations reveal that only spherical aberrations occur for all tested systems, however with an increased magnitude compared to the previous simulations producing parallel light output at the last lens (data not shown). For example, for a laser beam 8.3 mm in diameter focused 1 m behind the last lens, SA for the CT and the DK1 increase by $\approx 60\%$ compared to the case when the light is parallel. In contrast, the DK2 lens design shows only an increase in SA of 16%. Importantly, in absolute numbers the DK2 design still has 126 \times (13 \times) more aberration than the CT (DK1).

In contrast, if only the lateral trap position is modified (by tilting the incoming light with respect to the optical axis before entering the lens system), the amount of SA stays constant, but other primary aberrations like coma, astigmatism, field curvature and distortion increase significantly for the two simulated

DK (DK1, DK2) designs (data not shown). However due to the special combination of two positive lenses with one negative, the CT is able to correct these wavefront aberrations, resulting in 20–30 \times less aberrations compared to the two DK lens systems. Based on our simulation results for various beam magnifications and axial and lateral trap positions, we conclude that the CT shows in each case the least amount of primary aberrations compared to the DK setup.

Please note, if both axial and lateral trap positions should be steerable at the same time, a second CT and a third lens pair must be added to the proposed CT and DK lens design, respectively. In this scenario, the first CT (DK lens pair 1 and 2) controls beam magnification and axial trap position, and the second CT (DK lens pair 3) projects the conjugate focal plane of the system to the back aperture of the microscope objective to control the lateral trap position. Due to its superior off-axis performance in terms of aberrations, the CT arrangement provides an improved trap stiffness across the entire field of view.

To validate our simulation results for a 4 \times beam magnification, we acquire experimental interferograms for the DK1 [Fig. 2(c)] and CT [Fig. 2(d)] configurations using the integrated Twyman–Green interferometer. Both interferograms show an interference pattern without any circular substructure, indicating a plane and aberration-free wavefront which is in agreement with interferograms from our simulations. The various diameters of the circular pattern are explained by a different phase shift between the trapping beam and reference beam during image acquisition. Furthermore, the faint lines superimposing the interferogram are coherent noise originating from interference of the laser beam with the glass plate positioned in front of the camera chip.

After demonstrating the ability of the compact CT to change the trap position and to realize continuous beam magnifications over a wide range, without introducing primary aberrations, we now determine the trap stiffness for 1 and 2 μm PS particles and compare the resulting values to those obtained from the DK1 lens design. To maintain comparability, we align both setups to produce parallel light output with a beam diameter of $2\omega_0 = 4$ mm, using the Twyman–Green interferometer. For validation of this parameter, we determine the beam diameter at the exit pupil of the objective using a beam profiler camera [Figs. 3(a) and 3(b)]. For the DK setup [DK1, Fig. 3(a)], we find a symmetric Gaussian intensity profile (orange line in smaller panels) with $2\omega_{0,x} = (3.85 \pm 0.36)$ mm and $2\omega_{0,y} = (3.95 \pm 0.11)$ mm. We obtain a similar beam profile for the CT [Fig. 3(b), $2\omega_{0,x} = (3.98 \pm 0.17)$ mm, $2\omega_{0,y} = (3.88 \pm 0.23)$ mm]. On average, this corresponds to a filling ratio $\alpha = 0.84$. To measure the trap stiffness for each lens system, we trap a particle and sample its position signal ($f_{\text{Sample}} = 65536$ Hz) for 0.125 s at different axial trap positions above the coverslip. Subsequently, we fit an average power spectrum as an average of 32 independent spectra using a custom-written LabVIEW program that provides the trap stiffness k_x, k_y [20,21]. The fit range is set to 10–10,000 Hz, and we repeat this procedure 100 \times for each height and particle size for at least three particles.

For 1 μm PS particles, we first observe the maximum trap stiffness 4 μm above the coverslip [Fig. 3(c), CT: blue squares, DK1: black spheres] for both traps, an optimum that is in agreement with what has been reported previously for our immersion oil/objective combination [14]. Second, we find the

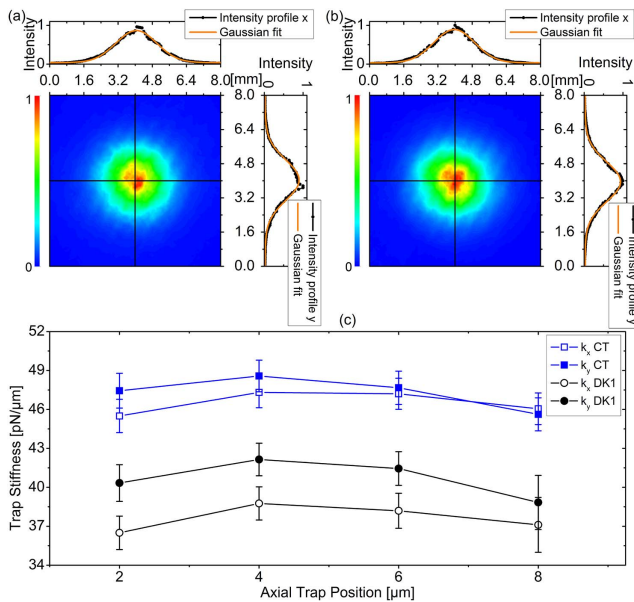


Fig. 3. Experimental measurements of the beam profile of the parallel trapping beam magnified by (a) the DK1 and (b) the CT at the exit pupil of the microscope objective. Both beams possess a symmetric Gaussian intensity profile with a similar beam diameter. (c) Experimentally measured lateral trap stiffness for 1 μm polystyrene beads in the optical trap formed by the DK1 (open and full black spheres) and the CT (open and full blue squares). In both cases, the trap stiffness peaks at a height of 4 μm above the coverslip, with the CT forming a stronger trap. To retrieve trap stiffness values, we averaged 3200 independent power spectra for each height and particle ($n = 3$).

trap stiffness k_y , in average to be 5% stronger than k_x . This is explained by the laser polarization dependence of the trap stiffness [23]. Third, the CT produces a $\approx 19\%$ stronger trap with a maximum trap stiffness of $k_{x,CT} = (47.3 \pm 1.2)$ pN/ μm and $k_{y,CT} = (48.6 \pm 1.2)$ pN/ μm compared to $k_{x,DK1} = (38.8 \pm 1.3)$ pN/ μm and $k_{y,DK1} = (42.1 \pm 1.3)$ pN/ μm of the DK1. However, in this context we must mention that for a filling ratio $\alpha = 0.84$, small changes in the beam diameter, and therefore in α , have a pronounced effect on the trap stiffness [12]. As an example, decreasing the beam diameter $2\omega_0$ from 4 to 3.8 μm (corresponding to an reduction in α from 0.84 to 0.8) lead to an 8.5% increase in trap stiffness. Despite the strong correlation between small changes in α and the trap stiffness, the CT lens design forms a well-defined trap that performs equally well or better than the commonly used DK setup. Fourth, by trapping 2 μm PS beads, we observe a $\approx 14\%$ stronger trap for the CT compared to the DK1. This is in agreement with our measurement for the 1 μm particles.

In essence, we proposed a versatile CT lens design as the centerpiece of an OT setup. We showed that a three-lens CT is capable of producing continuous beam magnifications over a broad range while tuning the axial and lateral trap position without changing lenses, focusing light in between lenses, or introducing primary aberrations. We achieved optimal lens alignment by integrating a Twyman–Green interferometer into the beam path. By trapping microparticles of various size, we demonstrated that the CT forms an equally strong trap

compared to a commonly used DK design but reduces the lens system length significantly. We think this CT design will be a significant advantage for novel implementations of OT such as laser tweezers assisted Raman spectroscopy [4] and optical trap based 3D displays [8], in which size, stability, and efficiency of the used OT setup are crucial to achieve optimal results.

Funding. Deutsche Forschungsgemeinschaft (DFG); Kempstiftelserna (JCK-1622).

Acknowledgment. T. S. acknowledges financial support from the German Research Foundation (DFG) via a postdoctoral fellowship. This work was supported by Kempstiftelserna to M. A.

REFERENCES

1. A. Ashkin, J. M. Dziedzic, J. E. Bjorkholm, and S. Chu, *Opt. Lett.* **11**, 288 (1986).
2. K. Svoboda, C. F. Schmidt, B. J. Schnapp, and S. M. Block, *Nature* **365**, 721 (1993).
3. S. B. Smith, Y. Cui, and C. Bustamante, *Science* **271**, 795 (1996).
4. C. Xie, M. A. Dinno, and Y.-Q. Li, *Opt. Lett.* **27**, 249 (2002).
5. J. P. Michel, I. L. Ivanovska, M. M. Gibbons, W. S. Klug, C. M. Knobler, G. J. L. Wuite, and C. F. Schmidt, *Proc. Natl. Acad. Sci. USA* **103**, 6184 (2006).
6. L. Bintu, T. Ishibashi, M. Dangkulwanich, Y. Y. Wu, L. Lubkowska, M. Kashlev, and C. Bustamante, *Cell* **151**, 738 (2012).
7. C. N. Spaulding, H. L. Schreiber, W. Zheng, K. W. Dodson, J. E. Hazen, M. S. Conover, F. Wang, P. Svenmarker, A. Luna-Rico, O. Francetic, M. Andersson, S. Hultgren, and E. H. Egelman, *eLife* **7**, e31662 (2018).
8. D. E. Smalley, E. Nygaard, K. Squire, J. Van Wagoner, J. Rasmussen, S. Gneiting, K. Qaderi, J. Goodsell, W. Rogers, M. Lindsey, K. Costner, A. Monk, M. Pearson, B. Haymore, and J. Peatross, *Nature* **553**, 486 (2018).
9. W. M. Lee, P. J. Reece, R. F. Marchington, N. K. Metzger, and K. Dholakia, *Nat. Protoc.* **2**, 3226 (2007).
10. M. Mahamdeh, "High resolution optical tweezers optimized for biological studies," Ph.D. dissertation (Technischen Universität Dresden, 2011).
11. M. Mahamdeh, C. Pérez Campos, and E. Schäffer, *Opt. Express* **19**, 11759 (2011).
12. A. Samadi and N. S. Reihani, *Opt. Lett.* **35**, 1494 (2010).
13. S. N. S. Reihani, M. A. Charsooghi, H. R. Khalesifard, and R. Golestanian, *Opt. Lett.* **31**, 766 (2006).
14. S. N. S. Reihani and L. B. Oddershede, *Opt. Lett.* **32**, 1998 (2007).
15. R. Kingslake and R. Barry Johnson, *Lens Design Fundamentals*, 2nd ed. (Academic, 2010), pp. 419–437.
16. H. Gross, H. Zügge, M. Peschka, and F. Blechinger, *Handbook of Optical Systems, Aberration Theory and Correction of Optical Systems* (2015), Chap. 29, pp. 1–70.
17. D. Malacara, *Optical Shop Testing* (Wiley, 2007).
18. M. Andersson, E. Fällman, B. E. Uhlin, and O. Axner, *Biophys. J.* **91**, 2717 (2006).
19. E. Fällman, S. Schedin, J. Jass, M. Andersson, B. E. Uhlin, and O. Axner, *Biosens. Bioelectron.* **19**, 1429 (2004).
20. S. F. Tolic-Nørrelykke, E. Schäffer, J. Howard, F. S. Pavone, F. Jülicher, and H. Flyvbjerg, *Rev. Sci. Instrum.* **77**, 103101 (2006).
21. J. Zakrisson, B. Singh, P. Svenmarker, K. Wiklund, H. Zhang, S. Hakobyan, M. Ramstedt, and M. Andersson, *Langmuir* **32**, 4521 (2016).
22. T. Dahlberg and T. Stangner, "Electronic supplementary information," Figshare (2018) [retrieved 8 February 2018], https://figshare.com/articles/Supplementary_Information/5863596.
23. A. Rohrbach, *Phys. Rev. Lett.* **95**, 168102 (2005).